08

The effect of Co and Ni on magnetic properties and microstructure of $BaFe_{12-x}Ni_xO_{19}$ and $BaFe_{12-x}Co_xO_{19}$ powders synthesized by the hydrothermal method

© V.G. Kostishin,[1] A.Yu. Mironovich,[1] H.I. Al-Khafaji,[1] G.A. Skorlupin,[1] E.S. Savchenko,[1] A.I. Ril[2]

[1] National University of Science and Technology, „MISiS“,
119049 Moscow, Russia
[2] Kurnakov Institute of General and Inorganic Chemistry, Russian Academy of Sciences,
119991 Moscow, Russia
e-mail: amironovich24@gmail.com

Received October 28, 2024
Revised December 9, 2024
Accepted December 9, 2024

In this work, nanoscale powders of Co- and Ni-substituted barium hexaferrites were obtained by hydrothermal synthesis ($BaFe_{12-x}Co_xO_{19}$ and $BaFe_{12-x}Ni_xO_{19}$ with $x = 0.1,\ 0.3,\ 0.5$). The obtained samples were analyzed by several methods, including XRD, EDX, VSM, FTIR and TEM. It is shown that despite the close chemical nature of Co^{2+} and Ni^{2+}, the effect of substitution of Fe^{3+} by these elements is completely different. Thus, nickel has virtually no effect on the shape and size of the resulting $BaFe_{12-x}Ni_xO_{19}$ particles (plate-shaped crystallites with a diameter of about 200 nm and a thickness of 60 nm). With an increase in the nickel concentration, the magnetic parameters of the resulting ferrites decrease almost linearly. Cobalt, on the contrary, in a certain concentration leads to a significant change in the morphology of the particles (thinning of the crystallites to 30 nm or less), resulting in a sharp decrease in the coercive force of the resulting powders. This effect is due to the fact that cobalt promotes the formation of the $BaFe_{12-x}Co_xO_{19}$ phase directly during the hydrothermal treatment of the precursors, whereas additional high-temperature treatment is required to form $BaFe_{12-x}Ni_xO_{19}$ and $BaFe_{12}O_{19}$.

Keywords: barium hexaferrite, hydrothermal synthesis, substituted hexaferrite, Mössbauer spectroscopy, magnetic measurements.

DOI: 10.61011/0000000000

Introduction

M-type barium hexaferrite (BaM) is a complex oxide with the stoichiometric formula $BaFe_{12}O_{19}$ or $BaO{\cdot}6Fe_2O_3$ and a structure that can be attributed to a spatial group $P6_3/mmc$ [1]. This material has been widely used in various fields of technology since 1952, when the Dutch company Philips introduced it as a new material under the name ferroxdure [2]. Studies of this material remains relevant today despite the long history of the use of BaM.

The properties of materials are known to depend on the material chemical composition which provides an option of their controllable variation. In this regard, a common method of material modification is isomorphic substitution — replacement of atoms or molecules with similar ones in size, shape, and electronic configuration. This strategy is applied to a wide range of materials [3–7], including hexaferrites [8–13]. In the structure of M-type hexaferrite, ferric ions are distributed over five different sub-lattices: 12*k*, 2*a*, 2*b*, $4f_1$ and $4f_2$. Magnetic moments of Fe^{3+} are oriented along the hexagonal *c* axis: at positions 12*k*, 2*a* and 2*b* in one direction („upward“ spin), and at positions $4f_1$ and $4f_2$ — in reverse direction („downward“ spin). Cations of different metals have some „preferred“ positions, depending on their type and synthesis conditions [14]. Thus, ferrites of the same chemical composition may have different parameters due to different distribution of cations across the sub-lattices. This leads to a variety of combinations of synthesis methods and replacement elements, which makes it possible to obtain materials with unique characteristics.

In this paper, the effect of iron substitution on cobalt or nickel in barium hexaferrite synthesized by the hydrothermal method is investigated. This method of synthesis has not been widely used so far for substituted ferrites, so the results obtained can be described as new findings. Additionally, $Fe^{3+} \rightarrow Co^{2+}$ and $Fe^{3+} \rightarrow Ni^{2+}$ substitutions themselves are relatively rare [14]. This is due to the fact that in such heterovalent substitutions, to sustain the charge balance the co-doping with tetravalent ions [15,16] is usually used, which facilitates synthesis, but distorts the effect of Co and Ni directly on the properties of ferrites.

1. Experiment

Barium hexaferrite powders were synthesized by hydrothermal method. A mixture of aqueous solution of $Fe(NO_3)_3 \cdot 9H_2O$, $Ba(NO_3)_2$ and $Co(NO_3)_2 \cdot 6H_2O$ (or $Ni(NO_3)_2 \cdot 6H_2O$) with aqueous solution of NaOH in the ratio of 60 to 20 ml, respectively, was used as a precursor. The solutions were prepared in such a way that in the

total volume (80 ml) the concentration of ions ($Fe^{3+} + Co^{2+}$ (or Ni^{2+})) was 0.25 M, the ratio (Fe + Co (or Ni))/Ba was 9, and the ratio OH^-/NO_3^- was equal 2.5. The ratio of Co (or Ni) to Fe was calculated using chemical formulae $BaCo_xFe_{12-x}O_{19}$ and $BaNi_xFe_{12-x}O_{19}$ ($x = 0.0$, 0.1, 0.3, 0.5). The prepared solutions were mixed in a 100 ml Teflon beaker, which was sealed in a steel autoclave and placed in an oven. The autoclave was slowly heated to 180 °C for 2 h and maintained at this temperature for 4 h. The separation of the sediment and the liquid solution was carried out by decantation, followed by washing the sediment with distilled water until reaching pH 7. Further, the sediment was dried at 90 °C for 8 h and ground into powder. After that the powders were annealed in the air at 900 °C for 1 h (the heating temperature was 15 °C/min).

X-ray diffraction analysis (XRD) was conducted in the Centre of Shared Equipment of IGIC RAS using Bruker D8 Advance diffractometer (emission of CuK_α, $\lambda = 0.154$ nm, $U = 40$ kV, $I = 40$ mA). Before the measurement, a crushed silicon crystal was added to the samples as a reference for calculating the lattice parameters. The obtained X-ray diffraction data was analyzed by Rietveld method using Profex software package [17]. The magnetic parameters of the samples were measured using JDAW-2000D vibration magnetometer. JEOL JEM-2100 transmission electron microscope (TEM) was used to study the microstructure of the samples. Infrared Fourier spectroscopy data was recorded using InfraLUM FT-08 infrared spectrometer. Element mapping and energy dispersion spectra were obtained using Bruker Quantax 75 scanning electron microscope (accelerating voltage of 15 kV, emission current 46.9 μA).

2. Results and discussion

X-ray diffraction patterns of the obtained samples were shown in Fig. 1. The results of samples analysis by Rietveld method are presented in Table 1. Hexaferrite of M-type and silicon are the major phases in all samples, however, on diffraction patterns of Ni-substituted ferrites there's a low-intensity reflex on 28.3°, that can be attributed to Barium monoferrite $BaFe_2O_4$ [18]. The presence of two phases with different ratio Fe/Ba ($BaFe_2O_4$ and $BaFe_{12}O_{19}$) may be confirmed by method of element mapping. Indeed, in $BaFe_{12-x}Ni_xO_{19}$ samples, the distribution of Fe and Ba is non-uniform — there are areas enriched in Ba that coincide with areas deficient in Fe (Fig. 2). Thus, it may be stated that if Ni^{2+} ions are present in the precursor it contributes to formation of a side phase of $BaFe_2O_4$.

According to the results of diffraction pattern analysis, the substitution of with for nickel or cobalt leads to a decrease in the lattice volume of hexaferrite (Table 1). At that, both Co^{2+}, and Ni^{2+} have ionic radius larger than that of Fe^{3+} [19], so the decrease in lattice was not expected. This effect may be related to the formation of oxygen vacancies that occur during such heterovalent substitutions to maintain the charge balance [14,20]. It is also impossible to exclude the possibility of oxidation of nickel and cobalt to the trivalent state, in which their ionic radii are already less than those of Fe^{3+}. According to the research findings [21–23], the hydrothermal treatment of products of reaction of Co^{2+} salts with bases leads to formation of Co_3O_4, i.e. to oxidation of part of initial Co^{2+} ions to Co^{3+}. At the same time, similar studies using Ni^{2+} salts more often demonstrate the formation of NiO, i.e., preservation of Ni^{2+} valence state [24–26].

Anyway, in these circumstances, it is necessary to confirm the presence of cobalt and nickel in the samples, for which an elemental analysis of the samples was carried out, the results of which are shown in Fig.3 and in Table.2. Since the amount of Ni or Co in the samples is less than 2 at.%, it is relatively difficult to detect them. However, correct scaling on spectra provides the peak values of Co$-K_{\beta_1}$ (7.649 keV) and Ni$-K_{\alpha_1}$ (7.478 keV) demonstrating the presence of these elements. At the same time, the amount of nickel in all cases is less than expected, and the amount of cobalt is higher than expected. This difference can be explained by assuming, based on the data from [21–26], that under synthesis conditions Co^{2+} is oxidized to Co^{3+}, and Ni^{2+} retains its valence. In this case Co^{3+} may better be constructed into the $BaFe_{12}O_{19}$ lattice compared to Ni^{2+}.

Co and Ni have different effects on the width of some hexagonal ferrite reflexes, and, accordingly, on the average crystallite sizes. Thus, the introduction of nickel has practically no effect on these parameters, while at a certain concentration of cobalt, the crystallite sizes decrease sharply in the direction of [001] (Table 1).

Powder of barium hexaferrite obtained by hydrothermal synthesis often consist of individual crystallites [20,27,28], therefore, physical dimensions of grains may match the dimensions calculated from diffraction patterns. However, the most reliable information can be obtained only by direct observation on electron microscope (Fig. 4). As can be seen, the actual particle sizes differ slightly from the calculated ones. Nevertheless, the trends observed for the calculated sizes coincide with those directly observed in the experiment: there are no noticeable changes with the growth of Ni concentration, whereas the addition of Co leads to a decrease in the thickness of the ferrite plates.

More fine structural differences can be detected using IR spectroscopy. The IR spectra of ferrites are shown in Fig. 5. The observed absorption bands are provided in Table 3. The characteristic absorption bands for barium hexaferrite M-type: 430−440, 535−546, 570−592 and 888−900 cm^{-1} [29–33]. Thus, the observed bands 538, 567 and 897 cm^{-1} may be unambiguously attributed to barium hexaferrite. According to [32], the peak of about 505 cm^{-1} corresponds to the oscillation of Fe−O bond in $4f_1$ site of the hexaferrite lattice. The band at 430−440 cm^{-1} was not observed in the spectra, but it can be shifted to 415 cm^{-1} due to the nanostructured state of ferrite [30]. A peak of about 415 cm^{-1} was also observed in the spectra of fine hexaferrite particles

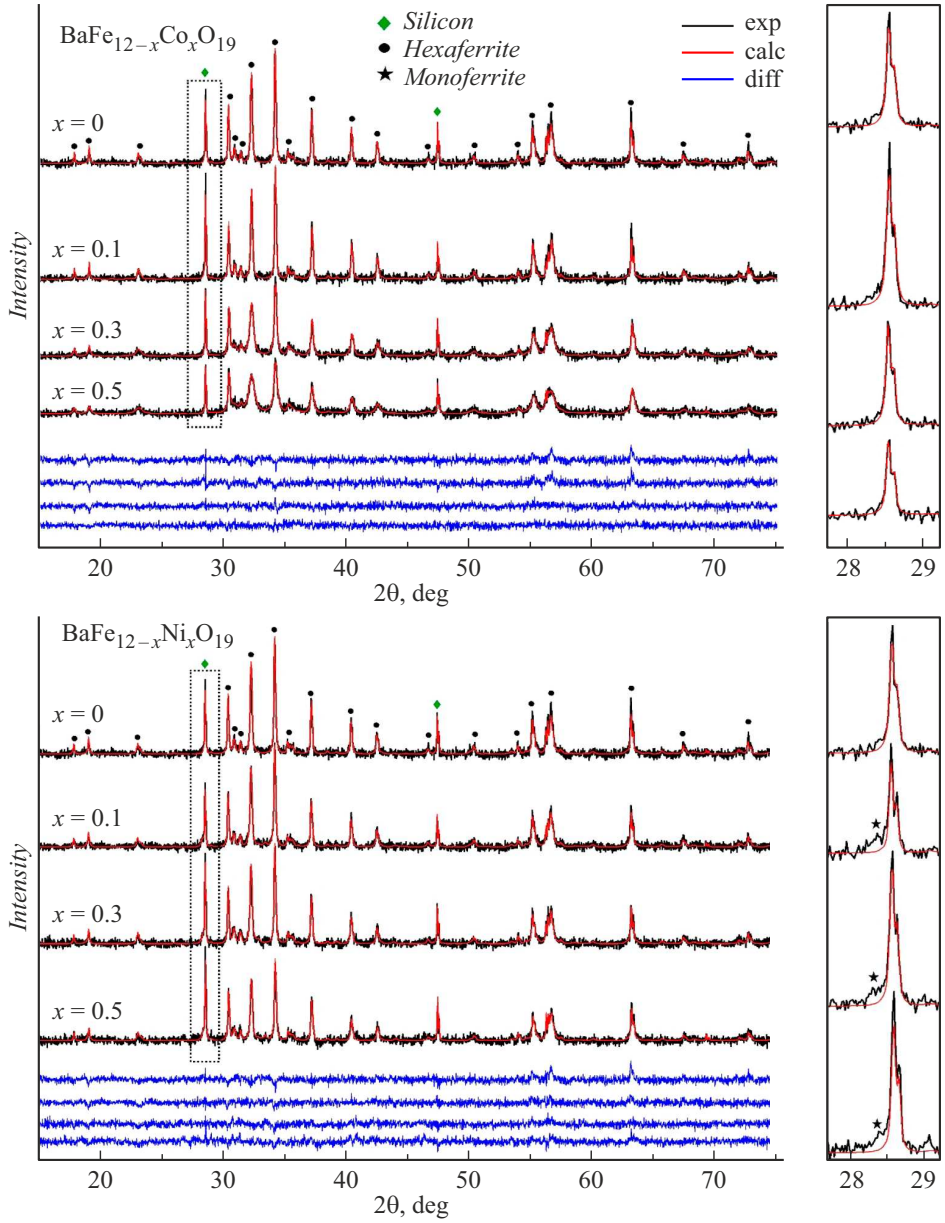

Figure 1. X-ray diffraction patterns of synthesized powders of $BaFe_{12-x}Ni_xO_{19}$ and $BaFe_{12-x}Co_xO_{19}$.

Table 1. Parameters of refinement of synthesized hexaferrite powders diffraction patterns using Rietveld method

Contents of substituting element, formula units	0	Ni			Co		
		0.1	0.3	0.5	0.1	0.3	0.5
R_{wp}, %	2.01	1.95	1.85	2.05	2.05	1.8	1.83
R_{exp}, %	1.73	1.78	1.72	1.76	1.77	1.74	1.76
χ^2	1.35	1.2	1.16	1.36	1.34	1.07	1.08
*a, Å	5.893	5.891	5.891	5.890	5.892	5.886	5.887
*c, Å	23.208	23.209	23.211	23.210	23.202	23.211	23.211
V, Å^3	697.957	697.513	697.573	697.306	697.539	696.39	696.626
**Average size of crystallite [001], nm	61	52	53	50	60	21	13
**Average size of crystallite [100], nm	97	91	95	87	105	73	54

Note. * — analysis error is ±0.001 Å, ** — calculated according to Profex algorithms

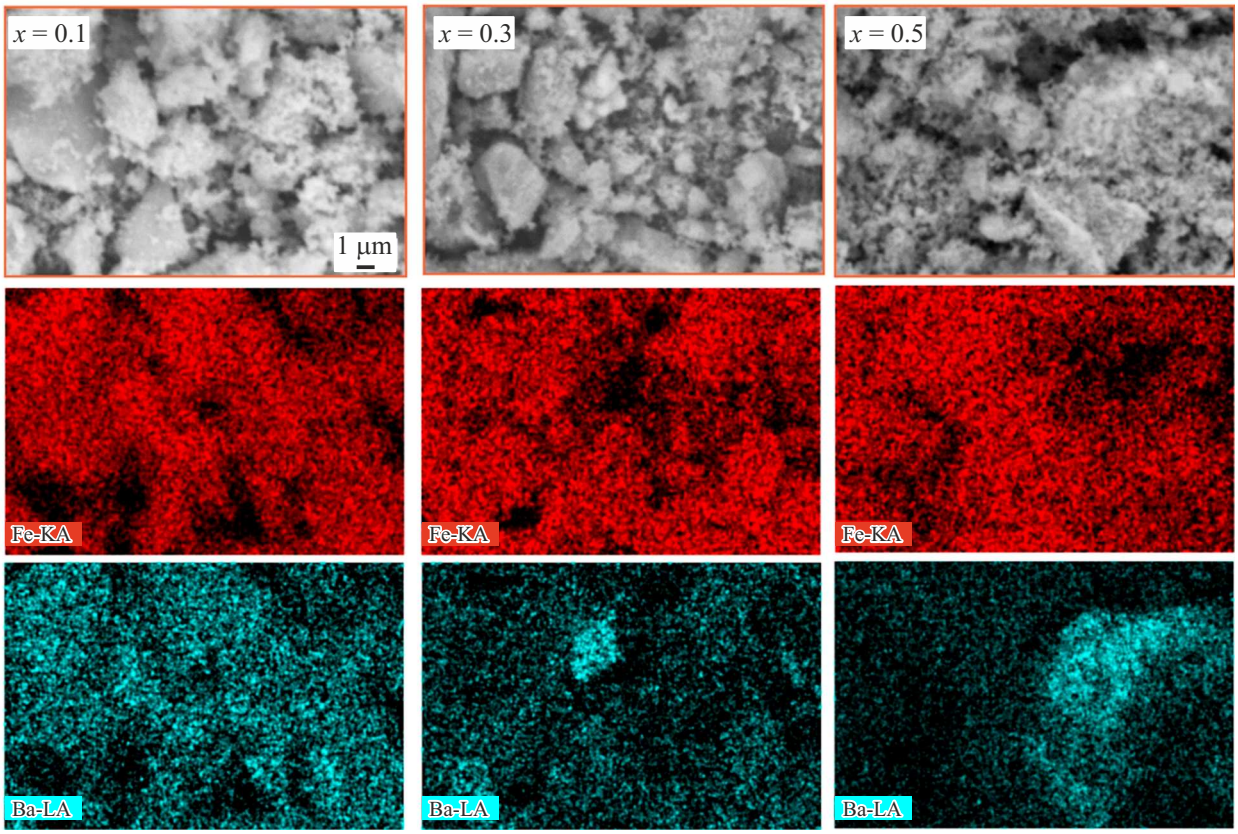

Figure 2. Fe and Ba distribution in samples $BaFe_{12-x}Ni_xO_{19}$.

Table 2. Results of quantitative analysis of energy dispersion spectra of samples

Sample	O, at.%	Fe, at.%	Ba, at.%	Co measured (expected), at.%	Ni measured (expected), at.%
$BaFe_{12}O_{19}$	60.45	36.43	3.12	–	–
$BaFe_{11.9}Co_{0.1}O_{19}$	58.11	37.34	3.75	0.8 (0.31)	–
$BaFe_{11.7}Co_{0.3}O_{19}$	58.25	36.21	3.89	1.65 (0.94)	–
$BaFe_{11.5}Co_{0.5}O_{19}$	57.61	37.1	3.14	2.15 (1.56)	–
$BaFe_{11.9}Ni_{0.1}O_{19}$	60.15	36.51	3.14	–	0.2 (0.31)
$BaFe_{11.7}Ni_{0.3}O_{19}$	49.62	44.23	5.39	–	0.76 (0.94)
$BaFe_{11.5}Ni_{0.5}O_{19}$	58.33	35.78	4.54	–	1.34 (1.56)

in studies [34,35]. The band 670 cm^{-1} is observed only for $BaFe_{12-x}Ni_xO_{19}$ spectra. This peak may be related to oscillations of Ni–O bonds, since it corresponds to one of the characteristic bands of Nickel oxide (678, 624 and 552 cm^{-1} [36]). The band 770 cm^{-1} may be attributed to $BaFe_2O_4$ [37] or $BaCO_3$ impurities [35]. It should be noted that this band disappears with the increase of cobalt concentration and does not depend on the nickel content. The same tendencies were observed for $BaFe_2O_4$ on diffraction patterns, therefore, the band 770 cm^{-1} was attributed to this phase. The band 858 cm^{-1} together with a wide doublet 1450 cm^{-1} was caused by the presence of $BaCO_3$ impurity [38]. Finally, the bands 1113, 1042, and 996 cm^{-1} in the spectrum of unsubstituted hexaferrite may be associated with an admixture of silicon, [39], which entered the sample during preparation of the latter for XRD. It should be noted that with the growth of cobalt concentration, the shape of the spectra changes, namely, the shoulders at 440–470 cm^{-1} and 620–650 cm^{-1} disappear. As mentioned above, the shape of the spectrum is influenced by the microstructure of ferrite [30]. In this case, the observed transformations of the spectra may be associated with a decrease in the average particle size caused by an increase in the cobalt content.

Table 3. Characteristic frequencies of IR radiation absorption by the obtained samples

Contents of substituting element, formula units	0	Ni			Co			Interpretation
		0.1	0.3	0.5	0.1	0.3	0.5	
Wavenumber, cm^{-1}	415	418	414	414	416	417	419	Fe–O (hexaferrite)
	505	503	503	505	506	–	–	Fe–O (hexaferrite)
	538	539	539	540	539	543	542	Fe–O (hexaferrite)
	567	570	570	572	569	571	570	Fe–O (hexaferrite)
	–	667	668	667	–	–	–	Ni–O
	770	771	770	770	773	767	–	Ba–O ($BaFe_2O_4$)
	858	858	858	859	858	858	859	Carbonate
	897	899	899	896	895	900	896	Ba–O (hexaferrite)

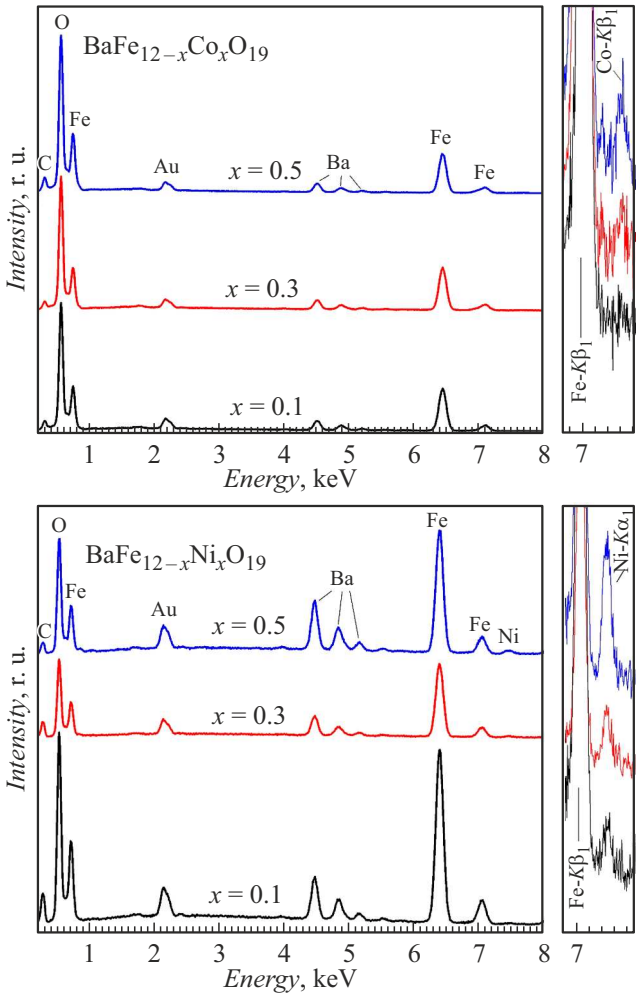

Figure 3. Energy-dispersive spectra of powders $BaFe_{12-x}Co_xO_{19}$ and $BaFe_{12-x}Ni_xO_{19}$.

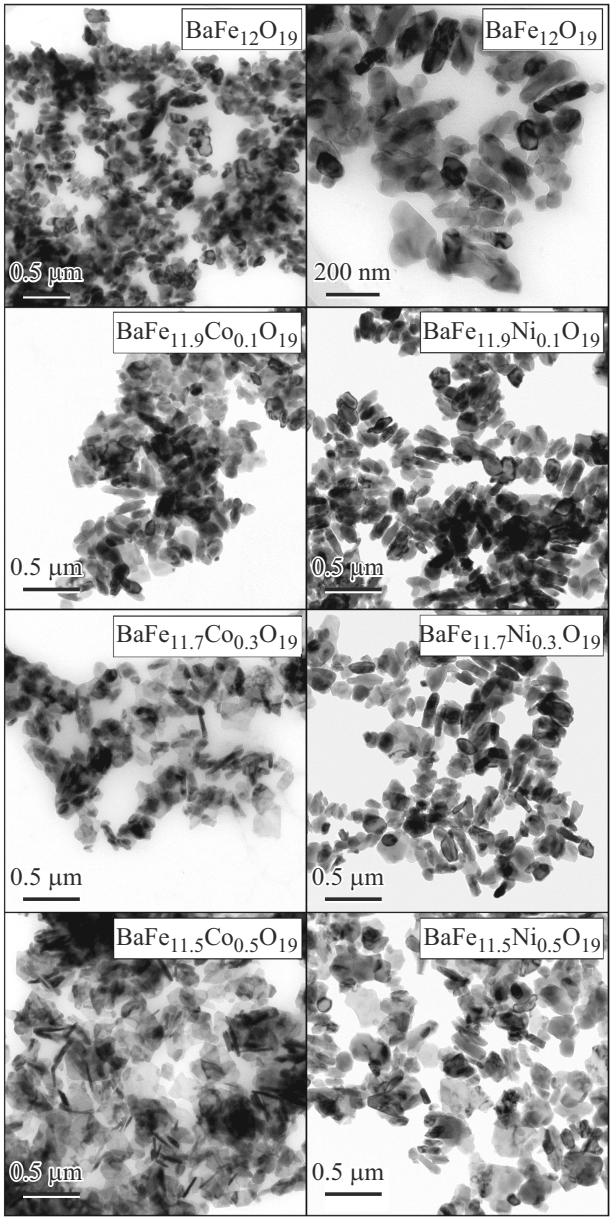

Figure 4. TEM images of powders $BaFe_{12-x}Co_xO_{19}$ and $BaFe_{12-x}Ni_xO_{19}$.

The results of magnetic measurements of the synthesized samples are shown in Fig. 6 and 7. As can be seen, the coercive force H_c of samples decreases with the growth of cobalt and nickel concentration, except for $BaFe_{11.9}Co_{0.1}O_{19}$ powder. Yet, the values of H_c are relatively (high more

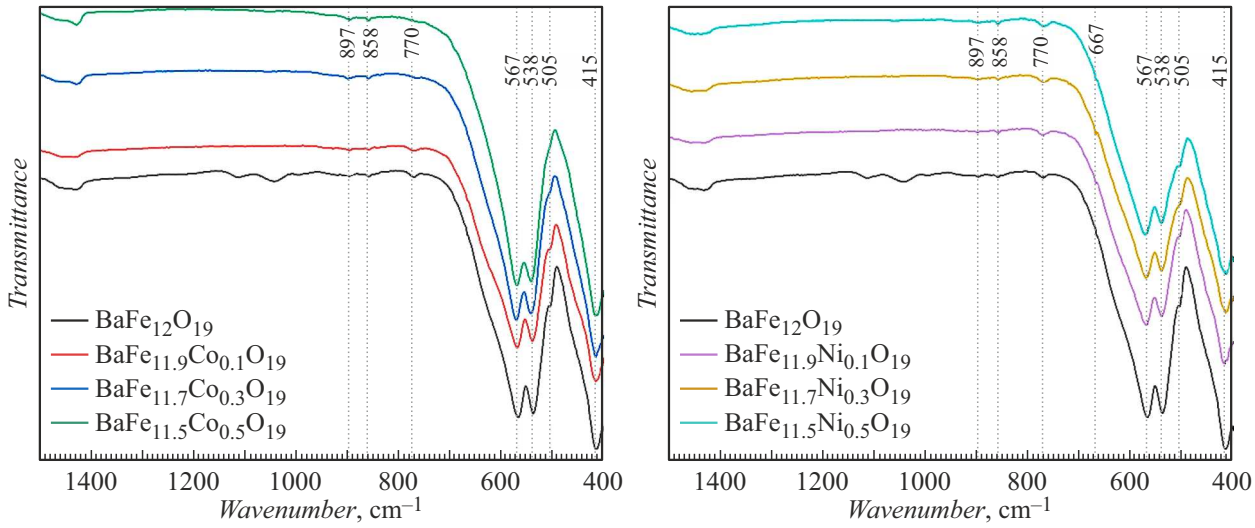

Figure 5. IR-spectra of ferrites $BaFe_{12-x}Ni_xO_{19}$ and $BaFe_{12-x}Co_xO_{19}$.

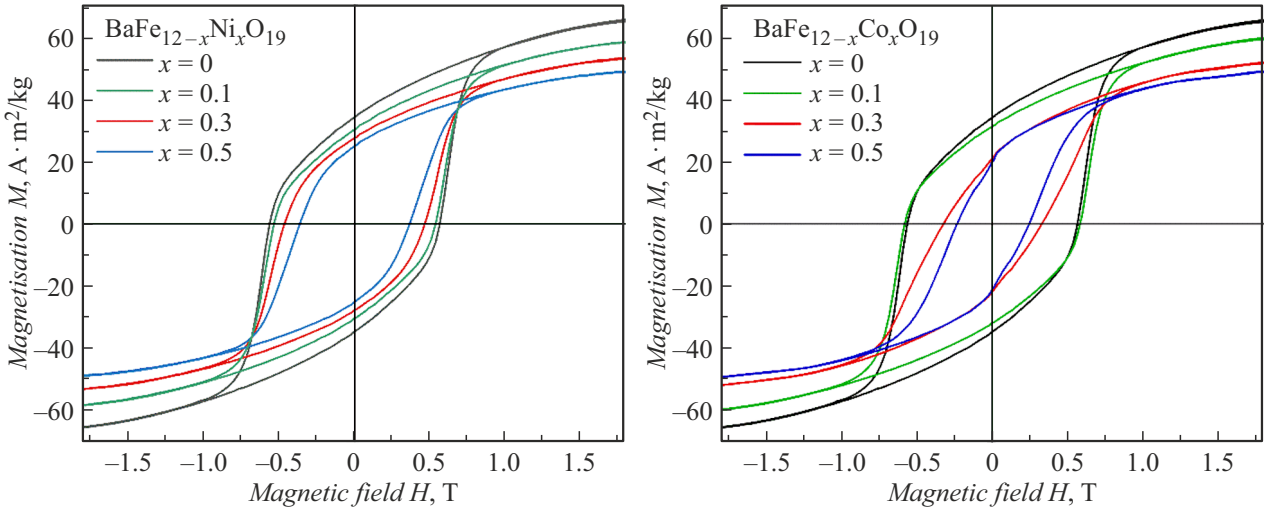

Figure 6. The magnetic hysteresis loops of $BaFe_{12-x}Ni_xO_{19}$ and $BaFe_{12-x}Co_xO_{19}$.

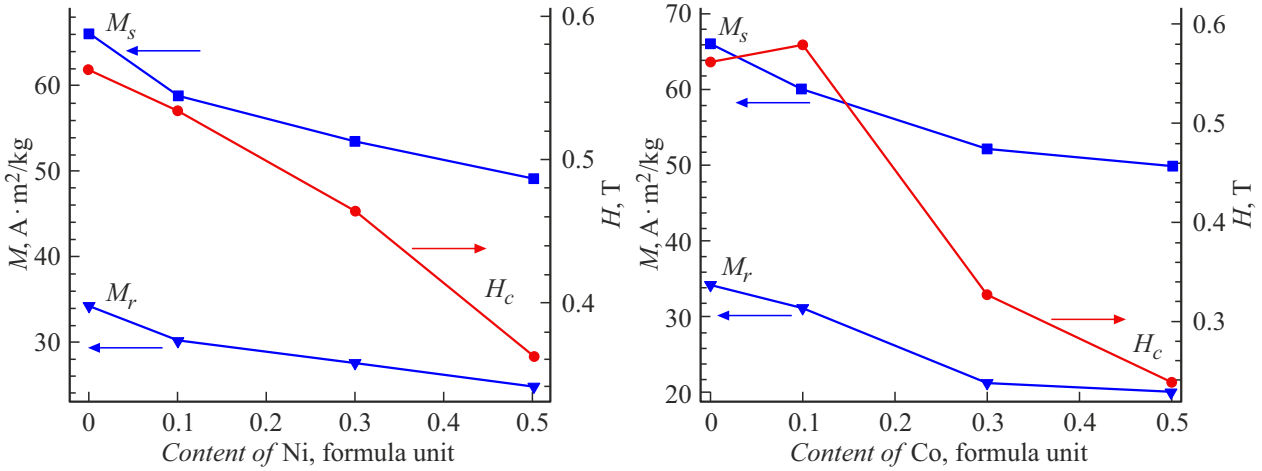

Figure 7. Magnetic parameters of samples $BaFe_{12-x}Ni_xO_{19}$ and $BaFe_{12-x}Co_xO_{19}$.

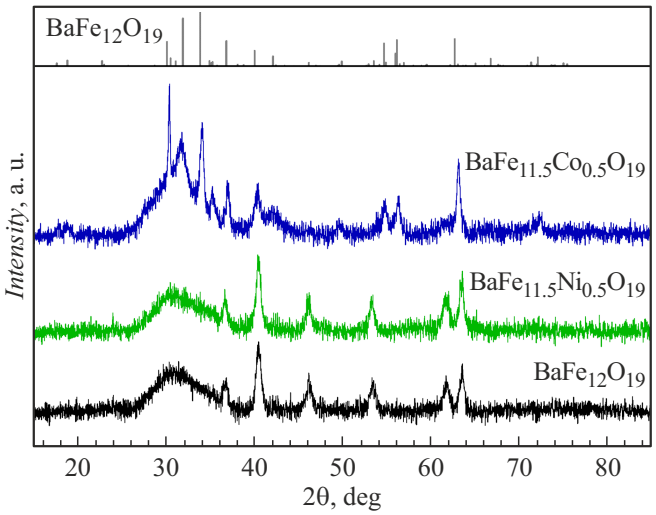

Figure 8. Diffraction patterns of samples $BaFe_{12}O_{19}$, $BaFe_{11.5}Ni_{0.5}O_{19}$ and $BaFe_{11.5}Co_{0.5}O_{19}$, obtained from the hydrothermal synthesis without high-temperature annealing.

than 0.25 T) which can be related to small sizes of particles and their single domain state.

Saturation magnetization also decreases with increasing of cobalt or nickel content. Cobalt and nickel ions (both in bivalent and trivalent forms) have a lower magnetic moment than Fe^{3+}. Thus, a decrease in magnetization is expected in cases of predominant occurrence of cobalt or nickel in structural positions with „upward" spin. In addition, saturation magnetization may decrease due to presence of the antiferromagnetic phase $BaFe_2O_4$ in the samples.

In case of Co-substituted ferrites, the decrease in magnetic parameters may be more related to changes in particles size than to the concentration of cobalt in the lattice. As can be seen, a drastic decrease of H_c in $BaFe_{12-x}Co_xO_{19}$ samples occurs simultaneously with particles thinning with concentration of Cobalt ($x > 0.1$). This behavior is consistent with the known dependences of hexaferrite coercive force on the ratio of the particle diameter to its thickness [40].

To determine how cobalt ions lead to such significant changes in the morphology of ferrite crystallites and, consequently, their magnetic properties, some powders were studied after hydrothermal treatment (before high-temperature annealing). Fig. 8 illustrates diffraction patterns of $BaFe_{12}O_{19}$, $BaFe_{11.5}Ni_{0.5}O_{19}$ and $BaFe_{11.5}Co_{0.5}O_{19}$ samples, and Fig. 9 — their micrographs. The diffraction pattern of $BaFe_{12}O_{19}$ sample shows that hydrothermal treatment under such conditions does not lead to the formation of ferrite, as a result of which additional annealing is performed at 900 °C. The positions of the reflexes of the obtained powder correspond to ferrihydrite — iron hydroxide with a non clearly identified composition. The presence of nickel in the solution did not lead to significant changes, and ferrihydrite was also obtained as a result of hydrothermal treatment. Cobalt, on the contrary, promoted the formation of hexaferrite nanoparticles without the need for further annealing. Thus, the sizes of particles $BaFe_{12}O_{19}$ (and $BaFe_{12-x}Ni_xO_{19}$) differ from sizes $BaFe_{12-x}Co_xO_{19}$ due to the fact that the first ones are formed during annealing of ferrihydrite (due to its agglomeration and dehydration), and the second one is formed directly from hydrothermal treatment of initial solution. At the same time, according to the micrographs and the amorphous halo on the diffraction pattern, ferrihydrite is also present in the non-annealed powder $BaFe_{11.5}Co_{0.5}O_{19}$.

Conclusion

In this study the powders of $BaFe_{12-x}Co_xO_{19}$ and $BaFe_{12-x}Ni_xO_{19}$ ($x = 0, 0.1, 0.3, 0.5$) were prepared by hydrothermal method followed by annealing. The resulting particles had a lamellar shape with a width of no more than 200 nm and a thickness of no more than 60 nm. The addition of nickel had virtually no effect on the morphology of the particles and led to the formation of a side phase of $BaFe_2O_4$. Cobalt, on the contrary, significantly affected the shape and size of the resulting hexaferrite crystallites and did not cause the formation of undesirable compounds.

Magnetic parameters $BaFe_{12-x}Ni_xO_{19}$ (saturation magnetization, coercive force and residual magnetization) decreased almost linearly with the growth of x from 0.1 to 0.5. At that the values of coercive force made more than 0.35 T. Such values are certainly related to the morphology and single domain state of the particles, which, in turn, are determined by the synthesis conditions.

Dependence of magnetic parameters of $BaFe_{12-x}Co_xO_{19}$ on x is more complex because of a drastic fall of H_c at $x > 0.3$. The decrease in H_c is probably due to a change in the morphology of crystallites with an increase in cobalt concentration — a more than two-fold thinning of lamellar crystallites.

The differences in the microstructure and magnetic properties of ferrites $BaFe_{12-x}Co_xO_{19}$ and $BaFe_{12-x}Ni_xO_{19}$ are resulting from a poor impact of nickel ions on ferrite formation processes: as a result of hydrothermal treatment of precursor solutions of $BaFe_{12-x}Ni_xO_{19}$ and $BaFe_{12}O_{19}$ the ferrihydrite is formed which is then transformed into barium hexaferrite after high-temperature annealing with formation of ferrite particles of a certain fraction. The presence of cobalt ions in the precursor solution leads to the fact that hexaferrite particles $BaFe_{12-x}Co_xO_{19}$ begin to form directly in the reactor during hydrothermal treatment, and their initially smaller sizes do not change significantly after high-temperature annealing.

Funding

This study was supported by a grant from the Russian Science Foundation (project No. 24-13-00268).

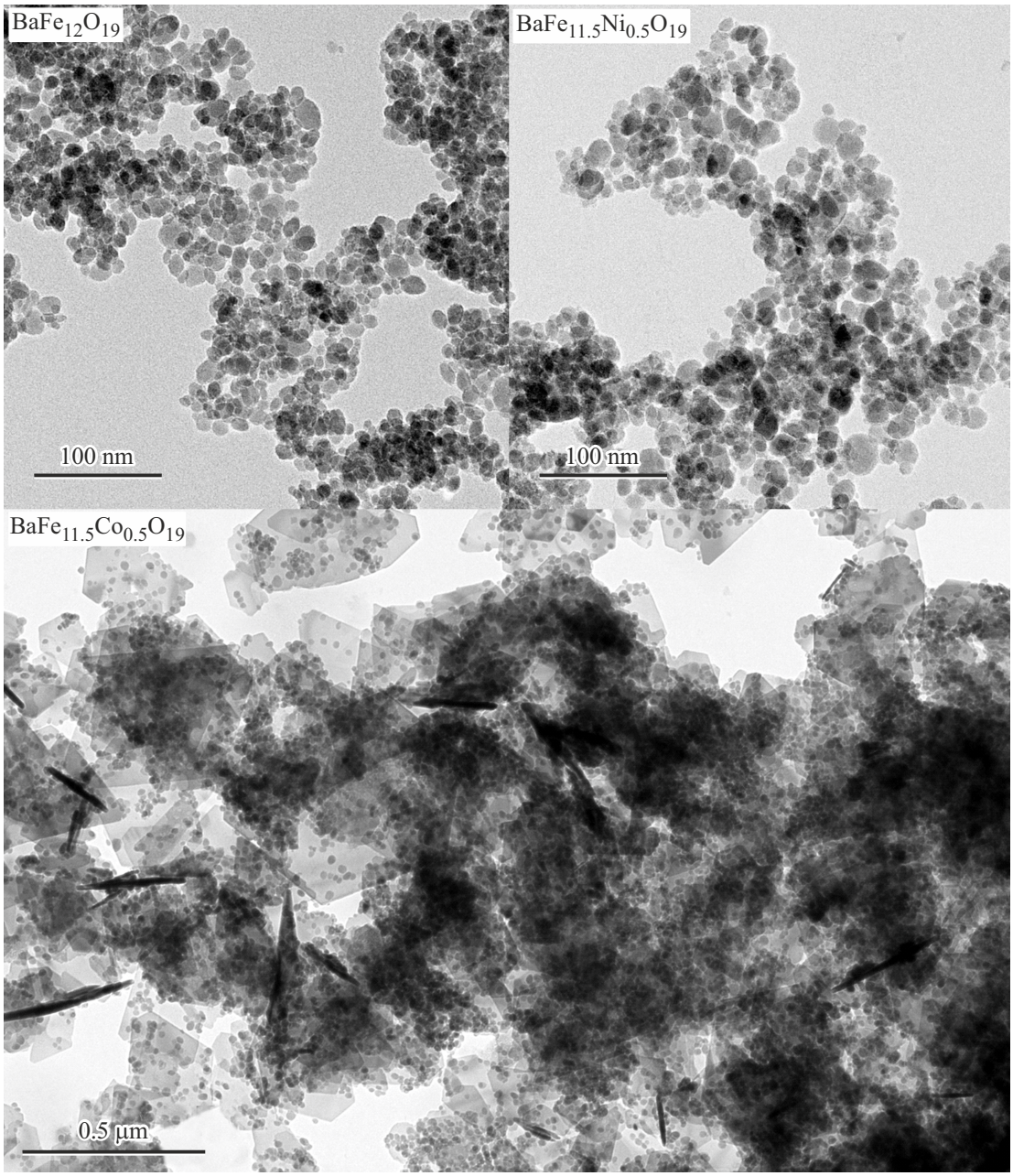

Figure 9. TEM images of powders $BaFe_{12}O_{19}$, $BaFe_{11.5}Ni_{0.5}O_{19}$ and $BaFe_{11.5}Co_{0.5}O_{19}$, obtained from the hydrothermal synthesis without high-temperature annealing.

Conflict of interest

The authors declare that they have no conflict of interest.

References

[1] R.C. Pullar. Progr. Mater. Sci., **57** (7), 1191 (2012). DOI: 10.1016/j.pmatsci.2012.04.001

[2] J.J. Went. Philips Techn. Rev., **13**, 194 (1952). DOI: 10.2497/jjspm.57.41

[3] R.I. Shakirzyanov, N.O. Volodina, A.L. Kozlovskiy, M.V. Zdorovets, D.I. Shlimas, D.B. Borgekov, Y.A. Garanin. J. Compos. Sci., **7** (10), 411 (2023). DOI: 10.3390/jcs7100411

[4] J.B. Baruah. Inorganica Chimica Acta, **560**, 121838 (2023). DOI: 10.1016/j.ica.2023.121838

[5] S. Prabhu, M. Maruthapandi, A. Durairaj, S. Arun Kumar, J.H. Luong, R. Ramesh, A. Gedanken. ACS Appl. Energy Mater., **6** (3), 1321 (2023). DOI: 10.1021/acsaem.2c03067

[6] E. van der Maas, T. Famprikis, S. Pieters, J.P. Dijkstra, Z. Li, S.R. Parnell, R.I. Smith, E.R.H. van Eck, S. Ganapathy, M. Wagemaker. J. Mater. Chem. A, **11** (9), 4559 (2023). DOI: 10.1039/D2TA08433C

[7] B. Sawicki, E. Tomaszewicz, M. Guzik, T. Gron, M. Oboz, H. Duda, S. Pawlus, P. Urbanowicz. Ceram. Intern., **49** (1), 944 (2023). DOI: 10.1016/j.ceramint.2022.09.068
[8] V.G. Kostishin, V.V. Korovushkin, K.V. Pokholok, A.V. Trukhanov, I.M. Isaev, A.Yu. Mironovich, M.A. Darwish. Phys. Solid State, **63** (11), 1680 (2021). DOI: 10.1134/S1063783421100176
[9] V.G. Kostishin, V.V. Korovushkin, I.M. Isaev, A.Yu. Mironovich, S.V. Trukhanov, V.A. Turchenko, K.A. Astapovich, A.V. Trukhanov. Phys. Solid State, **63**, 253 (2021). DOI: 10.1134/S106378342102013X
[10] V.V. Korovushkin, A.V. Trukhanov, V.G. Kostishin, I.M. Isaev, S.V. Trukhanov, K.A. Astapovich, A.Yu. Mironovich. Inorganic Mater., **56**, 707 (2020). DOI: 10.1134/S0020168520070080
[11] Y. Yang, S. Feng, X. Kan, Q. Lv, A.V. Trukhanov, S.V. Trukhanov. Chem. Select, **6** (3), 470 (2021) DOI: 10.1002/slct.202002620
[12] W. Zhang, J. Li, S. Yi, P. Zu, J. Wu, J. Lin, M. Li, W. Su. J. Alloys Compounds, **871**, 159563 (2021). DOI: 10.1016/j.jallcom.2021.159563
[13] Y. Slimani, B. Unal, M.A. Almessiere, A.D. Korkmaz, A. Baykal. Mater. Chem. Phys., **260**, 124162 (2021). DOI: 10.1016/j.matchemphys.2020.124162
[14] D.A. Vinnik, D.A. Zherebtsov, L.S. Mashkovtseva, S. Nemrava, A.S. Semisalova, D.M. Galimov, S.A. Gudkova, I.V. Chumanov, L.I. Isaenko, R. Niewa. J. Alloys Compounds, **628**, 480 (2015). DOI: 10.1016/j.jallcom.2014.12.124
[15] C. Liu, X. Kan, F. Hu, X. Liu, S. Feng, J. Hu, W. Wang, K.M.U. Rehman, M. Shezad, C. Zhang, H. Li, S. Zhou, Q. Wu. J. Alloys Compounds, **784**, 1175 (2019). DOI: 10.1016/j.jallcom.2019.01.112
[16] K. Pubby, S.B. Narang, S.K. Chawla, P. Kaur. J. Superconductivity Novel Magnetism, **30**, 3465 (2017). DOI: 10.1007/s10948-017-4141-2
[17] N. Doebelin, R. Kleeberg. J. Appl. Crystall., **48** (5), 1573 (2015). DOI: 10.1107/S1600576715014685
[18] M.C. Dimri, H. Khanduri, P. Agarwal, J. Pahapill, R. Stern. J. Magn. Magn. Mater., **486**, 165278 (2019). DOI: 10.1016/j.jmmm.2019.165278
[19] R.D. Shannon, C.T. Prewitt. Acta Crystallographica Section B: Structural Crystallography and Crystal Chemistry, **25** (5), 925 (1969). DOI: 10.1107/S0567740869003220
[20] F.H. Gjørup, M. Saura-Múzquiz, J.V. Ahlburg, H.L. Andersen, M. Christensen. Materialia, **4**, 203 (2018). DOI: 10.1016/j.mtla.2018.09.017
[21] S.K. Tripathy, M. Christy, N.H. Park, E.K. Suh, S. Anand, Y.T. Yu. Mater. Lett., **62** (6–7), 1006 (2008). DOI: 10.1016/j.matlet.2007.07.037
[22] Y. Hao, A.S. Teja. J. Mater. Res., **18** (2), 415 (2003). DOI: 10.1557/JMR.2003.0053
[23] K. Kanie, Y. Tsujikawa, A. Muramatsu. Mater. Transactions, **58** (7), 1014 (2017). DOI: 10.2320/matertrans.M2017090
[24] L. Lin, T. Liu, B. Miao, W. Zeng. Mater. Lett., **102**, 43 (2013). DOI: 10.1016/j.matlet.2013.03.103
[25] S. Cao, W. Zeng, H. Long, H. Zhang. Mater. Lett., **159**, 385 (2015). DOI: 10.1016/j.matlet.2015.07.045
[26] S. Virgin Jeba, S. Sebastiammal, S. Sonia, A. Lesly Fathima. Inorganic and Nano- Metal Chemistry, **51** (10), 1431 (2020). DOI: 10.1080/24701556.2020.1837163
[27] M. Drofenik, I. Ban, D. Makovec, A. Žnidaršič, Z. Jagličić, D. Hanžel, D. Lisjak. Mater. Chem. Phys., **127** (3), 415 (2011). DOI: 10.1016/j.matchemphys.2011.02.037
[28] D. Primc, D. Makovec, D. Lisjak, M. Drofenik. Nanotechnology, **20** (31), 315605 (2009). DOI: 10.1088/0957-4484/20/31/315605
[29] Z. Mosleh, P. Kameli, M. Ranjbar, H. Salamati. Ceram. Intern., **40** (5), 7279 (2014). DOI: 10.1016/j.ceramint.2013.12.068
[30] Y. Li, A. Xia, C. Jin. Synthesis, J. Mater. Sci.: Mater. Electron., **27**, 10864 (2016). DOI: 10.1007/s10854-016-5195-9
[31] R.E. El Shater, E.H. El-Ghazzawy, M.K. El-Nimr. J. Alloys Compounds, **739**, 327 (2018). DOI: 10.1016/j.jallcom.2017.12.228
[32] W.Y. Zhao, P. Wei, X.Y. Wu, W. Wang, Q.J. Zhang. J. Appl. Phys., **103** (6), 3902 (2008). DOI: 10.1063/1.2884533
[33] S.M. El-Sayed, T.M. Meaz, M.A. Amer, H.A. El Shersaby. Phys. B: Condensed Matter., **426**, 137 (2013). DOI: 10.1016/j.physb.2013.06.026
[34] S. Ram. Phys. Rev. B, **51** (10), 6280 (1995). DOI: 10.1103/PhysRevB.51.6280
[35] S. Hasan, B. Azhdar. Results in Physics, **42**, 105962 (2022). DOI: 10.1016/j.rinp.2022.105962
[36] K. Sajilal, A.M.E. Raj. Optik, **127** (3), 1442 (2016). DOI: 10.1016/j.ijleo.2015.11.026
[37] J. Huang, H. Zhuang, W.L. Li. Mater. Res. Bull., **38** (1), 149 (2003). DOI: 10.1016/S0025-5408(02)00979-0
[38] X. Wang, Y. Ye, X. Wu, J.R. Smyth, Y. Yang, Z. Zhang, Z. Wang. Phys. Chem. Minerals, **46**, 51 (2019). DOI: 10.1007/s00269-018-0986-6
[39] S.A. Memon, W. Liao, S. Yang, H. Cui, S.F.A. Shah. Materials, **8** (2), 499 (2015). DOI: 10.3390/ma8020499
[40] O. Kubo, T. Ido, H. Yokoyama, Y. Koike. J. Appl. Phys., **57** (8), 4280 (1985). DOI: 10.1063/1.334585

Translated by T.Zorina